



BNL-228516-2025-JAAM

# Sm<sub>2</sub>Ru<sub>3</sub>Sn<sub>5</sub>: A Noncentrosymmetric Cubic Member of the Ln<sub>2</sub>M<sub>3</sub>X<sub>5</sub> Family

W. Brown, G. Kotliar

To be published in "Zeitschrift für anorganische und allgemeine Chemie"

May 2025

Condensed Matter Physics and Materials Science Department  
**Brookhaven National Laboratory**

**U.S. Department of Energy**

USDOE Office of Science (SC), Basic Energy Sciences (BES)

Notice: This manuscript has been authored by employees of Brookhaven Science Associates, LLC under Contract No. DE-SC0012704 with the U.S. Department of Energy. The publisher by accepting the manuscript for publication acknowledges that the United States Government retains a non-exclusive, paid-up, irrevocable, world-wide license to publish or reproduce the published form of this manuscript, or allow others to do so, for United States Government purposes.

## **DISCLAIMER**

This report was prepared as an account of work sponsored by an agency of the United States Government. Neither the United States Government nor any agency thereof, nor any of their employees, nor any of their contractors, subcontractors, or their employees, makes any warranty, express or implied, or assumes any legal liability or responsibility for the accuracy, completeness, or any third party's use or the results of such use of any information, apparatus, product, or process disclosed, or represents that its use would not infringe privately owned rights. Reference herein to any specific commercial product, process, or service by trade name, trademark, manufacturer, or otherwise, does not necessarily constitute or imply its endorsement, recommendation, or favoring by the United States Government or any agency thereof or its contractors or subcontractors. The views and opinions of authors expressed herein do not necessarily state or reflect those of the United States Government or any agency thereof.

**Zeitschrift für anorganische und allgemeine Chemie**  
**Sm<sub>2</sub>Ru<sub>3</sub>Sn<sub>5</sub>: A Non-centrosymmetric Cubic Member of the Ln<sub>2</sub>M<sub>3</sub>X<sub>5</sub> Family**  
--Manuscript Draft--

<b>Manuscript Number:</b>	
<b>Article Type:</b>	Research Article
<b>Corresponding Author:</b>	Julia Y. Chan, Ph.D. Baylor University Waco, Texas UNITED STATES OF AMERICA
<b>Corresponding Author E-Mail:</b>	Julia_Chan@baylor.edu
<b>Other Authors:</b>	W. Kice Brown Benny C. Schundelmier Hengxin Tan Corey Melnick Gabriel Kotliar Binghai Yan Kaya Wei Gregory T. McCandless
<b>Requested Editor:</b>	Thomas Fässler
<b>Keywords:</b>	Intermetallic compounds; Transition metals; Materials science; Samarium; Lanthanides
<b>Manuscript Classifications:</b>	Crystal growth; Magnetic properties; Materials science; Rare Earths
<b>Suggested Reviewers:</b>	Vincent Yannello The University of Tampa vyannello@ut.edu  Xin Gui University of Pittsburgh xig@pitt.edu  Riccardo Freccero University of Genoa Department of Chemistry and Industrial Chemistry: Universita degli Studi di Genova Dipartimento di Chimica e Chimica Industriale riccardo.freccero@unige.it  Sebastian Peter JNCASR: Jawaharlal Nehru Centre for Advanced Scientific Research sebastiancp@jncasr.ac.in  Claudia Felser Max-Planck-Institute for Chemical Physics of Solids: Max-Planck-Institut für Chemische Physik fester Stoffe claudia.felser@cpfs.mpg.de
<b>Opposed Reviewers:</b>	
<b>Abstract:</b>	We present an optimized synthetic method for Sm <sub>2</sub> Ru <sub>3</sub> Sn <sub>5</sub> and investigate its physical properties and electronic structure. Sm <sub>2</sub> Ru <sub>3</sub> Sn <sub>5</sub> was prepared by arc-melting stoichiometric ratios of the elements and confirmed by single crystal and powder X-ray diffraction. An antiferromagnetic transition was observed at TN = 3.8 K. A modified Curie-Weiss fit to the data in the range 50 - 150 K yielded a Curie-Weiss temperature: Θ <sub>CW</sub> = -36.6 K and an effective magnetic moment: μ <sub>eff</sub> = 0.83 μ <sub>B</sub> , in agreement with a Sm <sup>3+</sup> oxidation state. Field-dependent magnetization up to H = 7 T at 2 K showed a maximum response of 0.06 μ <sub>B</sub> , significantly lower than the expected Sm <sup>3+</sup> saturation moment (0.71 μ <sub>B</sub> ). Resistivity measurements indicate metallic behavior, and analysis of the magnetic entropy from the heat capacity revealed a doublet ground state due to

	crystal electric field splitting. The electronic structure and density of states were calculated with density function theory (DFT) and further supported by the local density approximation with dynamical mean-field theory (LDA+DMFT). Our experimental and computational results highlight localized Sm <sup>3+</sup> moments and suggest a possible interplay between Ruddelman-Kitel-Kasuya-Yosida (RKKY) and Kondo interactions, positioning Sm <sub>2</sub> Ru <sub>3</sub> Sn <sub>5</sub> as a promising material for studying topology and complex physical phenomena.
<b>Author Comments:</b>	We have no additional comments.
<b>Section/Category:</b>	Dedicated to Professor Gordon Miller on the Occasion of His 65th Birthday
<b>Additional Information:</b>	
<b>Question</b>	<b>Response</b>
Dedication	per email: Gordon Miller will celebrate his 65th birthday.
Do you agree to comply with the legal and ethical responsibilities outlined in the journal's Notice to Authors?	Yes
Has a previous version of this manuscript been submitted to this journal?	No
Is this manuscript, or part of it, currently under consideration elsewhere?	No
Is this manuscript, or part of it, published, posted, or in press? This includes content posted on preprint servers ( <a href="#">preprint guidelines</a> ) or published as part of a thesis.	No
Optional: please provide us with information about the history of your manuscript, including previous submissions, transfers, or prior versions:	This is the first submission of this manuscript.
Does the research described in this manuscript include animal experiments or human subjects or tissue samples from human subjects?	No
Do you or any of your co-authors have a conflict of interest to declare?	No



Click here to access/download  
**Supporting Information**  
2025Feb3\_Sm2Ru3Sn5\_SupplInfo.pdf



Click here to access/download  
**Supporting Information**  
[scxrd0480\\_298k\\_CheckCIFReport.pdf](#)



Click here to access/download  
**Supporting Information**  
[\*\*scxrd0586\\_160k\\_CheckCIFReport.pdf\*\*](#)

1  
2  
3  
4  
5

## Sm<sub>2</sub>Ru<sub>3</sub>Sn<sub>5</sub>: A Non-centrosymmetric Cubic Member of the Ln<sub>2</sub>M<sub>3</sub>X<sub>5</sub> Family

W. Kice Brown,<sup>1</sup> Benny C. Schundelmier,<sup>2,3</sup> Hengxin Tan,<sup>4</sup> Corey Melnick,<sup>5,6</sup> Gabriel Kotliar,<sup>5,6</sup> Binghai Yan,<sup>4</sup> Kaya Wei,<sup>2</sup> Gregory T. McCandless,<sup>1</sup> and Julia Y Chan<sup>\*1</sup>

<sup>1</sup> Department of Chemistry and Biochemistry, Baylor University, Waco, TX 76706, United States

<sup>2</sup> National High Magnetic Field Laboratory, Florida State University, Tallahassee, FL 32306, United States

<sup>3</sup> Department of Physics, Florida State University, Tallahassee, FL 32306, United States

<sup>4</sup> Department of Condensed Matter Physics, Weizmann Institute of Science, Rehovot 7610001, Israel

<sup>5</sup> Department of Physics and Astronomy, Rutgers University, Piscataway, NJ 08854, United States

<sup>6</sup> Department of Matter Physics and Materials Science, Brookhaven National Laboratory, Upton, NY 11973, United States

### Abstract

We present an optimized synthetic method for Sm<sub>2</sub>Ru<sub>3</sub>Sn<sub>5</sub> and investigate its physical properties and electronic structure. Sm<sub>2</sub>Ru<sub>3</sub>Sn<sub>5</sub> was prepared by arc-melting stoichiometric ratios of the elements and confirmed by single crystal and powder X-ray diffraction. An antiferromagnetic transition was observed at T<sub>N</sub> = 3.8 K. A modified Curie-Weiss fit to the data in the range 50 - 150 K yielded a Curie-Weiss temperature: θ<sub>CW</sub> = -36.6 K and an effective magnetic moment:  $\mu_{\text{eff}} = 0.83 \mu_B$ , in agreement with a Sm<sup>3+</sup> oxidation state. Field-dependent magnetization up to H = 7 T at 2 K showed a maximum response of 0.06  $\mu_B$ , significantly lower than the expected Sm<sup>3+</sup> saturation moment (0.71  $\mu_B$ ). Resistivity measurements indicate metallic behavior, and analysis of the magnetic entropy from the heat capacity revealed a doublet ground state due to crystal electric field splitting. The electronic structure and density of states were calculated with density function theory (DFT) and further supported by the local density approximation with dynamical mean-field theory (LDA+DMFT). Our experimental and computational results highlight localized Sm<sup>3+</sup> moments and suggest a possible interplay between Ruddelmann-Kitel-Kasuya-Yosida (RKKY) and Kondo interactions, positioning Sm<sub>2</sub>Ru<sub>3</sub>Sn<sub>5</sub> as a promising material for studying topology and complex physical phenomena.

**Keywords:** Intermetallic compounds, Transition metals, Materials science, Samarium, Lanthanides

1  
2  
3  
4  
5  
6  
7 **1. Introduction**

8  
9  
10  
11  
12  
13  
14  
15  
16  
17  
18  
19  
20  
21  
22  
23  
24  
25  
26  
27  
28  
29  
30  
31  
32  
33  
34  
35  
36  
37  
38  
39  
40  
41  
42  
43  
44  
45  
46  
47  
48  
49  
50  
51  
52  
53  
54  
55  
56  
57  
58  
59  
60  
61  
62  
63  
64  
65  
Intermetallic compounds with samarium (Sm) can exhibit a +2 or +3 oxidation state. Notable properties of Sm<sup>3+</sup> compounds include the Kondo effect in SmSn<sub>3</sub>,<sup>[1]</sup> heavy fermion behavior in Sm<sub>3</sub>Te<sub>4</sub>,<sup>[2]</sup> large magnetoresistance of over 100% at H = 9 T for SmPd<sub>2</sub>Ga<sub>2</sub>,<sup>[3]</sup> and multiple magnetic transitions are observed in Sm<sub>2</sub>Sn<sub>3</sub>.<sup>[4]</sup> A subset of Sm compounds are also recognized for their topology, where spin-orbit coupling (SOC) and *d-f* orbital hybridization can lead to nontrivial topological surface states. In SmB<sub>6</sub>, the combination of topology and SOC creates a strong spin-orbit torque without exclusive surface conduction, a property that is intrinsic to topological insulators.<sup>[5-6]</sup> Another example is SmS which exhibits a pressure-induced valence instability, fluctuating from a Sm<sup>2+</sup> to a Sm<sup>3+</sup> state at 6.5 kbar.<sup>[7]</sup> The change in valence is accompanied by a first-order phase transformation, where the high pressure golden phase (*g*-SmS) has a topological band structure containing Dirac cones.<sup>[8]</sup> SmCoIn<sub>5</sub> is another example of an intermediate-valent compound, where antiferromagnetic ordering dominates and Kondo coherence is not observed; however, charge fluctuations from the crystal field highlight a competition between Kondo and Ruderman-Kittel-Kasuya-Yosida (RKKY) interactions.<sup>[9]</sup> Finally, a large topological Hall effect was observed in the Weyl semimetal SmAlSi which can be varied with magnetic field, supporting a Weyl-mediated, spiral magnetic ordering.<sup>[10]</sup> Our interest in finding a compound with high symmetry, topology, and SOC was influenced by the aforementioned examples.

In our 2023 survey of the Ln<sub>2</sub>M<sub>3</sub>X<sub>5</sub> compounds (Ln = lanthanide, or actinide; M = transition metal; X = Si, Ga, Ge, In, Sn), eight different structure types were identified.<sup>[11]</sup> Recently, Ce<sub>2</sub>Au<sub>3</sub>In<sub>5</sub> was identified as a Weyl-Kondo semimetal.<sup>[12]</sup> The authors predicted a number of strongly correlated topological semimetals and experimentally validated Ce<sub>2</sub>Au<sub>3</sub>In<sub>5</sub> (space group # 31, *Pmn2*<sub>1</sub>). Of the Ln<sub>2</sub>M<sub>3</sub>X<sub>5</sub> family of compounds, consisting of over 230 analogues, at least 15 examples are reported to have polymorphism or structural phase transformations, particularly the analogues with Groups 8 and 9 transition metals. Our group has studied Pr<sub>2</sub>Co<sub>3</sub>Ge<sub>5</sub> which exhibits valence instability from nearly Pr<sup>4+</sup> to Pr<sup>3+</sup> upon a monoclinic to orthorhombic structural phase transition.<sup>[13]</sup> Another notable Ln<sub>2</sub>M<sub>3</sub>X<sub>5</sub> analogue is polymorphic Sm<sub>2</sub>Ru<sub>3</sub>Ge<sub>5</sub> that adopts both the tetragonal Sc<sub>2</sub>Fe<sub>3</sub>Si<sub>5</sub>

1  
2  
3  
4 and the orthorhombic  $U_2Co_3Si_5$  structure types,<sup>[14-15]</sup> where each polymorph has been  
5 linked to charge density wave behavior.<sup>[15-16]</sup> While both polymorphs exhibit  $Sm^{3+}$   
6 character, the magnetism of each manifests differently. The tetragonal polymorph exhibits  
7 a ferromagnetic transition at 7 K;<sup>[15]</sup> however, the orthorhombic polymorph of  $Sm_2Ru_3Ge_5$   
8 has an antiferromagnetic transition at 7 K.<sup>[17]</sup> Sm-containing compounds, particularly  
9 those adopting the  $Ln_2M_3X_5$  structures, offer a rich system to study complex structural  
10 and magnetic phenomena. For these reasons,  $Sm_2Ru_3Sn_5$  was chosen to be the focus of  
11 this study as a potential candidate for strongly correlated phenomena. While quite  
12 different from the other  $Ln_2M_3X_5$  structure types,  $Sm_2Ru_3Sn_5$  ( $a = 9.4606(8)$  Å;  $I\bar{4}3m$ )<sup>[18]</sup>  
13 adopts a structure that is a non-centrosymmetric variation from the binary cubic,  
14 centrosymmetric  $Ru_3Sn_7$  structure ( $a = 9.332$  Å;  $Im\bar{3}m$ ).<sup>[19]</sup> Since a topological band  
15 structure has been established for  $Ru_3Sn_7$  analogues,<sup>[20]</sup> an investigation into the  
16 noncentrosymmetric analogue could reveal new states that were unrealized in the  
17 centrosymmetric environment. Furthermore, there is no understanding on the impact of *f*-  
18 elements to physical properties of the  $Ru_3Sn_7$  structure type. Herein, we report an  
19 investigation of the synthesis, physical properties, and electronic structure of  $Sm_2Ru_3Sn_5$   
20 to understand the introduction of *f*-orbitals to the  $Ru_3Sn_7$  structure type.  
21  
22

23 **2. Results and Discussion**

24 **2.1. Synthesis**

25 A previous synthesis of  $Sm_2Ru_3Sn_5$  arc-melted and annealed samples at 600 °C for 30  
26 days, where Ru and  $SmRuSn_3$  impurities were observed in 15 wt% and 5 wt%,  
27 respectively.<sup>[18]</sup> Single crystals suitable for X-ray diffraction were isolated from the surface  
28 of the annealed samples. Similarly, we also synthesized  $Sm_2Ru_3Sn_5$  by arc-melting  
29 stoichiometric amounts of Sm, Ru, and Sn. Annealing seemed to have no impact on the  
30 formation of  $Sm_2Ru_3Sn_5$ ; however, an important experimental condition to the formation  
31 of  $Sm_2Ru_3Sn_5$  was the particle size of Ru used in the experiment. Larger pieces of Ru  
32 introduced inhomogeneous regions to the boule, resulting in areas of different  
33 stoichiometry that contributed to the formation of byproducts. Ru powder was vital for  
34 consistent formation of  $Sm_2Ru_3Sn_5$  without any byproducts. A small homogeneity range  
35 of formation was observed, and any deviation in stoichiometry from the 2:3:5 (Sm:Ru:Sn)  
36

1  
2  
3  
4 ratio results in the formation of  $\text{Ru}_2\text{Sn}_3$  and  $\text{SmRuSn}_3$  as impurities. Attempts to grow  
5 single crystals with the flux method from excess Sn led to the formation of  $\text{Ru}_3\text{Sn}_7$  and  
6  $\text{SmRuSn}_3$ , excess Ga or In flux led to the formation of both  $\text{RuX}_3$  and  $\text{SmX}_2$  (X = Ga, In),  
7 and excess Bi flux led to the formation of  $\text{Ru}_3\text{Sn}_7$  and  $\text{Ru}_2\text{Sn}_3$ .  
8  
9  
10  
11  
12

## 2.2. Crystal Structure

13  
14  
15  $\text{Sm}_2\text{Ru}_3\text{Sn}_5$  crystallizes in the cubic space group  $I\bar{4}3m$  (No. 217) with room temperature  
16 unit cell parameter:  $a = 9.4575(5)$  Å. Details of the single crystal data collection and  
17 refinement parameters are outlined in Table 1.  $\text{Sm}_2\text{Ru}_3\text{Sn}_5$  is an ordered  
18 noncentrosymmetric variant of the centrosymmetric  $\text{Ru}_3\text{Sn}_7$  structure, consistent with the  
19 previously reported lattice parameter  $a = 9.4606(8)$  Å.<sup>[18]</sup> The  $\text{Ru}_3\text{Sn}_7$  structure can be  
20 visualized as a collection of doubled, condensed square antiprisms that form  
21 interpenetrating frameworks (Figure 1a), consisting of three atomic positions: Ru1 (12e,  
22 4 m . m), Sn1 (12d,  $\bar{4}$  m . 2), and Sn2 (16f, . 3 m).<sup>[21-22]</sup> The doubled square antiprisms of  
23  $\text{Ru}_3\text{Sn}_7$  are connected by a Sn<sub>8</sub> cube with the Sn2 site at the vertices. To compare the  
24 Sn2 sites to the structure of  $\text{Sm}_2\text{Ru}_3\text{Sn}_5$ , the cube can also be described as two  
25 congruent, interpenetrating tetrahedra (Figure 1b). The crystal structure of  $\text{Sm}_2\text{Ru}_3\text{Sn}_5$   
26 consists of four atomic positions: Sm1 (8c, . 3 m), Ru1 (12e, 2 . m m), Sn1 (12d,  $\bar{4}$  . .),  
27 and Sn2 (8c, . 3 m), where the fractional atomic coordinates are outlined in Table 2. In  
28  $\text{Sm}_2\text{Ru}_3\text{Sn}_5$ , the tetrahedra are incongruent—one made from four Sn2 atoms and one  
29 made from four Sm1 atoms. This motif of two, interpenetrating  $\text{Ln}_4$  and  $\text{Sn}_4$  tetrahedra  
30 (Figure 1c) is also present in the  $\text{Ho}_5\text{Co}_6\text{Sn}_{18}$ , where the Ho tetrahedral sublattice is  
31 associated with geometric frustration, and the spins order noncollinearly.<sup>[23]</sup> While the  
32 distance between the Sm atoms in  $\text{Sm}_2\text{Ru}_3\text{Sn}_5$  are too far to be considered within bonding  
33 distance ( $d_{\text{Sm-Sm}} = 5.373(1)$  Å), it is comparable to the interatomic distance in the Ho(2)<sub>4</sub>  
34 tetrahedron ( $d_{\text{Ho-Ho}} = 5.06 - 5.15$  Å) for  $\text{Ho}_5\text{Co}_6\text{Sn}_{18}$ .  
35  
36  
37  
38  
39  
40  
41  
42  
43  
44  
45  
46  
47  
48  
49  
50  
51  
52  
53  
54  
55  
56  
57  
58  
59  
60  
61  
62  
63  
64  
65

1  
2  
3  
4 **Table 1. Single Crystal Data Collection and Refinement Parameters for Sm<sub>2</sub>Ru<sub>3</sub>Sn<sub>5</sub>**  
5

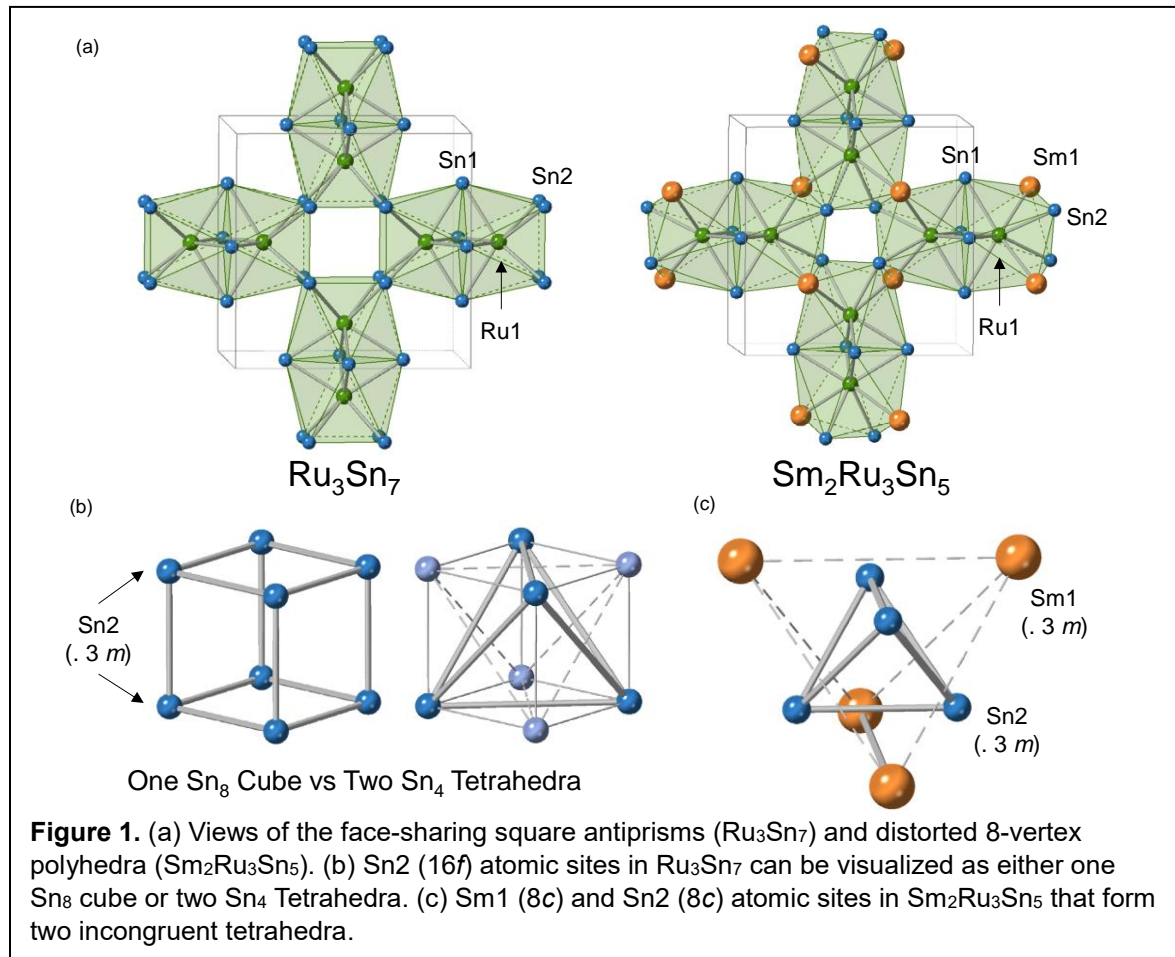
6 Formula	Sm <sub>2</sub> Ru <sub>3</sub> Sn <sub>5</sub>	
7 Space Group	<i>I</i> 43 <i>m</i>	
8 Temperature (K)	298	160
9 <i>a</i> (Å)	9.4575(5)	9.4438(6)
10 <i>V</i> (Å <sup>3</sup> )	845.92(13)	842.25(16)
11 <i>Z</i>	4	
12 <i>θ</i> (°)	3.1 - 30.5	
13 <i>μ</i> (mm <sup>-1</sup> )	33.23	33.37
14 Measured Reflections	19123	21240
15 Independent Reflections	272	272
16 <i>R</i> <sub>int</sub>	0.073	0.082
17 $\Delta\rho_{\text{max}}, \Delta\rho_{\text{min}}$ (e <sup>-</sup> /Å <sup>3</sup> )	0.57, -0.62	0.89, -1.11
18 <i>R</i> [ $F^2 > 2\sigma(F^2)$ ]	0.011	0.015
19 <i>wR</i> <sub>2</sub> ( $F^2$ )	0.024	0.030
20	$R = \sum  F_o  -  F_c  / \sum  F_o $	
21	$wR_2 = (\sum [w(F_o^2 - F_c^2)^2] / \sum [w(F_o^2)^2])^{1/2}$	

22 **Table 2. Fractional Atomic Coordinates and Displacement Parameters (T = 298 K)**  
23

32 Site	33 Wyckoff	34 <i>x</i>	35 <i>y</i>	36 <i>z</i>	37 <i>U</i> <sub>eq</sub> (Å <sup>2</sup> )
38 Sm1	8c	0.20088(4)	0.20088(4)	0.20088(4)	0.01085(15)
39 Ru1	12e	½	0.14990(8)	½	0.00727(16)
40 Sn1	12d	¼	0	½	0.00986(15)
41 Sn2	8c	0.38416(6)	0.38416(6)	0.38416(6)	0.00776(17)

42 Electron counting has been discussed in relation to the Ru<sub>3</sub>Sn<sub>7</sub> structure type as a way  
43 to rationalize the chemical composition of substituted analogues.<sup>[21, 24-25]</sup> For Sm<sub>2</sub>Ru<sub>3</sub>Sn<sub>5</sub>  
44 and Ru<sub>3</sub>Sn<sub>7</sub>, the valence electron concentrations are 50 (5 e<sup>-</sup>/atom) and 52 (5.2 e<sup>-</sup>/atom),  
45 respectively. While VEC is a useful tool to identify trends within a given structure type or  
46 class of intermetallics, normalization of VEC to the transition metal sites offers insight into  
47 the bonding.<sup>[25]</sup> When using the 18-*n*+*m* rule,<sup>[26]</sup> Ru<sub>3</sub>Sn<sub>7</sub> has 17.33 electrons/Ru.  
48 Assuming Sm<sup>3+</sup>, the VEC drops to 16.67 electrons/Ru in Sm<sub>2</sub>Ru<sub>3</sub>Sn<sub>5</sub>. The reduced VEC  
49 implies either an increase in the Ru—Ru bonding within the structure (the *n* term), or a  
50 reduced Sn—Sn interaction (the *m* term). A change in the degree of Ru—Ru bonding can  
51 be ruled out, since there is a minimal contraction of 0.064(2) Å for the Ru—Ru contacts  
52 in Sm<sub>2</sub>Ru<sub>3</sub>Sn<sub>5</sub> (compared to Ru<sub>3</sub>Sn<sub>7</sub>). Coupled with this change (shown in Figure 1) is a  
53

similar amount of expansion in the Sn2—Sn2 connectivity due to the replacement of half the Sn2 atoms (. 3 *m* site symmetry) in the Ru<sub>3</sub>Sn<sub>7</sub> structure with Sm (Sm<sub>2</sub>Ru<sub>3</sub>Sn<sub>5</sub>:  $d_{\text{tet}} = 3.100(6)$  Å; Ru<sub>3</sub>Sn<sub>7</sub>:  $d_{\text{cube}} = 3.020(1)$  Å). It is possible that the change in the *m* term is more heavily influenced by the introduction of Sm—Sn interactions ( $d_{\text{Sm1-Sn2}} = 3.004(5)$  Å) between adjacent tetrahedra; however, deviations from the ideal VEC could also be explained by a high density of states at the Fermi level. To further understand the impact of this structural distortion on the chemistry of Sm<sub>2</sub>Ru<sub>3</sub>Sn<sub>5</sub>, we investigated the physical properties and electronic structure.



### 2.3. Physical Properties

Figure 2 shows the magnetic susceptibility and field-dependent magnetization measurements of Sm<sub>2</sub>Ru<sub>3</sub>Sn<sub>5</sub>. An antiferromagnetic transition at  $T_N = 3.8$  K is observed (shown in Figure 2a). The inverse susceptibility (Figure 2b) shows a slight curvature that

1  
 2  
 3  
 4  
 5  
 6  
 7  
 8  
 9  
 10  
 11  
 12  
 13  
 14  
 15  
 16  
 17  
 18  
 19  
 20  
 21  
 22  
 23  
 24  
 25  
 26  
 27  
 28  
 29  
 30  
 31  
 32  
 33  
 34  
 35  
 36  
 37  
 38  
 39  
 40  
 41  
 42  
 43  
 44  
 45  
 46  
 47  
 48  
 49  
 50  
 51  
 52  
 53  
 54  
 55  
 56  
 57  
 58  
 59  
 60  
 61  
 62  
 63  
 64  
 65

is consistent with a temperature independent magnetic term. The magnetic susceptibility data was fit from 50 - 150 K with a modified Curie-Weiss law:  $\chi = \chi_0 + C/(T - \theta_{\text{CW}})$ , where the temperature-independent term:  $\chi_0 = 0.0026$ , C is the Curie constant, and the Curie-Weiss temperature:  $\theta_{\text{CW}} = -36.6$  K. The effective moment from the fit was  $0.83 \mu_B$ , consistent with the expected effective moment for  $\text{Sm}^{3+}$  ( $\mu_{\text{eff}} = 0.84 \mu_B$ ). In systems with strong spin-orbit coupling (SOC), the preferred alignment directions of spins can conflict with each other, causing the original Curie-Weiss law to break down from temperature-dependent local magnetic moments.<sup>[27]</sup> The combination of SOC and frustration could lead to fractionalization of fermionic excitations, known as a quantum spin liquid.<sup>[28]</sup> The modified Curie-Weiss law accounts for a more accurate  $\theta_{\text{CW}}$  by introducing a constant to better fit temperature-independent contributions to the data.  $\text{SmPd}_2\text{Al}_3$  is a compound with a strongly anisotropic magnetic response.<sup>[29]</sup> Subsequent magnetometry and neutron diffraction experiments illuminated a geometrically frustrated Sm lattice with

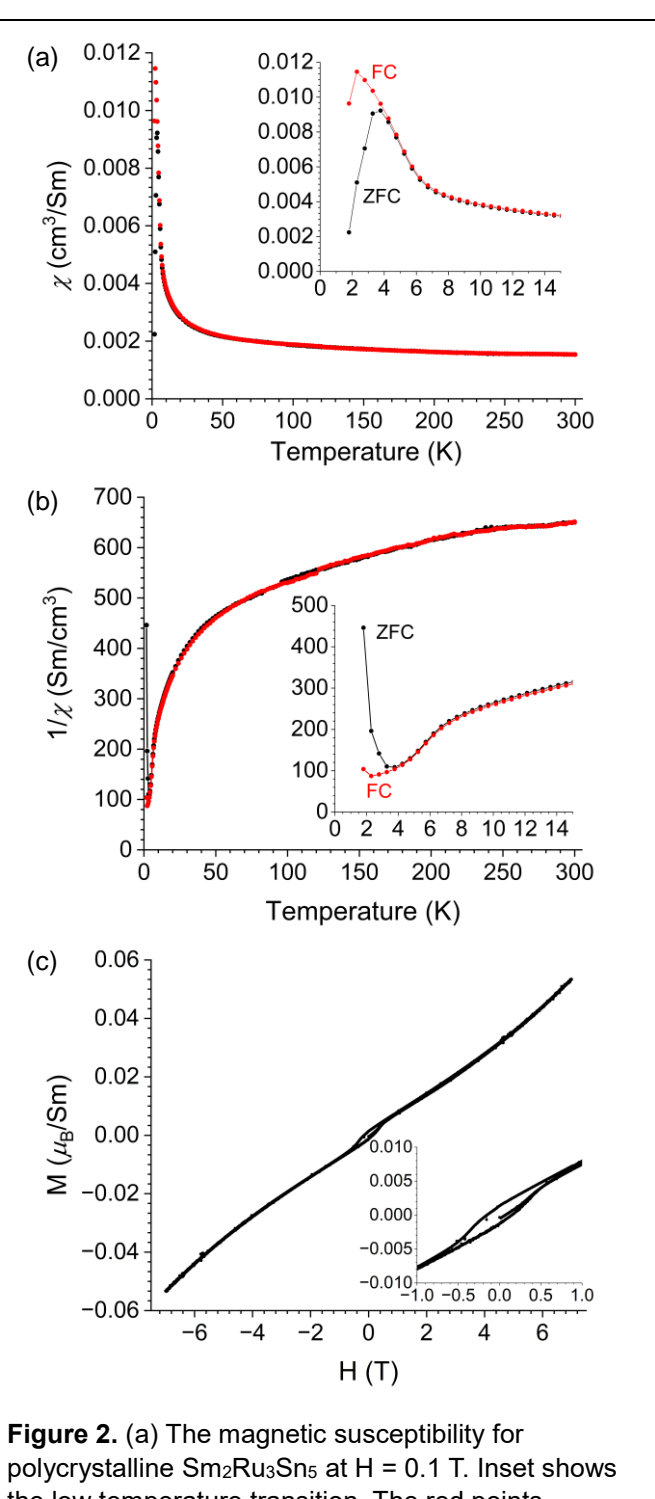
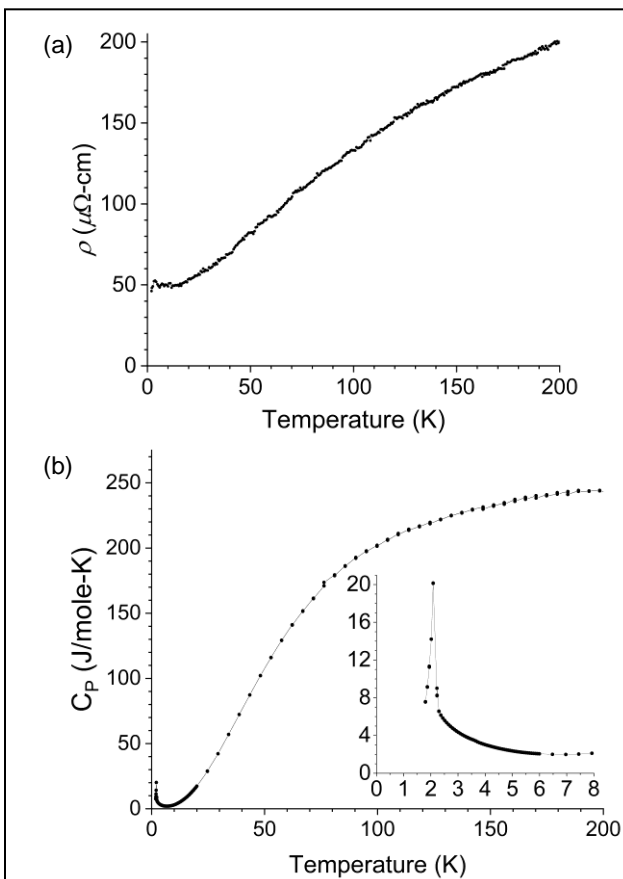


**Figure 2.** (a) The magnetic susceptibility for polycrystalline  $\text{Sm}_2\text{Ru}_3\text{Sn}_5$  at  $H = 0.1$  T. Inset shows the low temperature transition. The red points represent the field cooled (FC) experiment, and the black points represent the zero field cooled (ZFC) experiment. (b) The inverse of the magnetic susceptibility of  $\text{Sm}_2\text{Ru}_3\text{Sn}_5$ . (c) The field-dependent magnetization for  $\text{Sm}_2\text{Ru}_3\text{Sn}_5$  measured at  $T = 2$  K.

1  
2  
3  
4 complex magnetic behavior that is influenced by the kinetic effect of a sweeping magnetic  
5 field.<sup>[30]</sup> While  $\text{Sm}_2\text{Ru}_3\text{Sn}_5$  is cubic, directional dependence of interactions (anisotropy)  
6 can also cause frustration. Considering the frustration index ( $f = \theta_{\text{CW}}/T_N$ ),  $\text{Sm}_2\text{Ru}_3\text{Sn}_5$  has  
7 a value:  $f = 9.6$ . Even though a value of  $f > 5$  is accepted for frustrated  $3d$  transition metal  
8 magnets, similar values for  $4f$  magnets should be treated with caution as the  $\theta_{\text{CW}}$  may be  
9 potentially inflated due to crystal field effects.<sup>[31-32]</sup> An alternative explanation to the large  
10 difference between  $\theta_{\text{CW}}$  and  $T_N$  is that the Sm moments are screened by the conduction  
11 electrons. The phenomenon could be mediated by RKKY<sup>[33-34]</sup> or Kondo interactions.<sup>[35-36]</sup>  
12 These findings indicate  $\text{Sm}_2\text{Ru}_3\text{Sn}_5$  may be a good candidate to study low-temperature  
13 Kondo screening in a cubic, non-  
14 centrosymmetric environment. The MvH  
15 measurements (Figure 2c) were  
16 collected below the antiferromagnetic  
17 transition at 2 K and show a slight  
18 hysteresis at low fields as well as a small,  
19 field dependent response; however, no  
20 saturation was observed up to 7 T with a  
21 response that is an order of magnitude  
22 lower than the calculated saturation  
23 moment ( $0.71 \mu_B$ ).

24  
25  
26  
27  
28  
29  
30  
31  
32  
33  
34  
35  
36  
37  
38  
39  
40 The resistivity of  $\text{Sm}_2\text{Ru}_3\text{Sn}_5$  is shown in  
41 Figure 3a. The measured compound is  
42 metallic and has a slight curvature,  
43 similar to the shape of the resistivity for  
44  $\text{Ru}_3\text{Sn}_7$ .<sup>[37]</sup> The authors report the non-  
45 linearity of the resistivity in  $\text{Ru}_3\text{Sn}_7$  to be  
46 similar to the A15 ( $\text{Nb}_3\text{Sn}$ ) compounds  
47 and relate the curvature to the presence  
48 of  $d$ -orbitals near the Fermi level. The  
49 resistivity of  $\text{Sm}_2\text{Ru}_3\text{Sn}_5$  at room  
50 temperature is  $\sim 50 \mu\Omega\text{-cm}$ , which is  
51 higher than the reported value of  $\sim 10 \mu\Omega\text{-cm}$   
52 for  $\text{Ru}_3\text{Sn}_7$ .<sup>[37]</sup> The resistivity increases  
53 with temperature, reaching  $\sim 200 \mu\Omega\text{-cm}$  at  
54 200 K. The heat capacity of  $\text{Sm}_2\text{Ru}_3\text{Sn}_5$  is  
55 shown in Figure 3b. The heat capacity  
56 increases with temperature, reaching  
57  $\sim 250 \text{ J/mole-K}$  at 200 K. An inset  
58 shows a sharp feature at 2.1 K, consistent  
59 with the antiferromagnetic transition.  
60



61  
62  
63  
64  
65 **Figure 3.** (a) Temperature dependent electrical  
resistivity of a polished piece of polycrystalline  
 $\text{Sm}_2\text{Ru}_3\text{Sn}_5$  measured using a four-point probe  
method. (b) Temperature dependent heat capacity  
for  $\text{Sm}_2\text{Ru}_3\text{Sn}_5$  measured on the same sample.  
Inset shows a sharp feature at 2.1 K, consistent  
with the antiferromagnetic transition.

1  
2  
3  
4 temperature ( $\sim 200 \mu\Omega\text{-cm}$ ) is nearly three times that of the reported value for  $\text{Ru}_3\text{Sn}_7$  at  
5 room temperature ( $\sim 70 \mu\Omega\text{-cm}$ ). The more semimetallic character of  $\text{Sm}_2\text{Ru}_3\text{Sn}_5$  is  
6 consistent with the scattering of the conduction electrons due to a local magnetic moment.  
7 It is worth noting that another group recently studied the impact of Sb-doping on the  
8 resistivity of  $\text{Ru}_3\text{Sn}_7$ .<sup>[38]</sup> The authors found that when Sb was substituted for Sn in  
9  $\text{Ru}_3\text{Sb}_{1.75}\text{Sn}_{5.25}$ , superconductivity was observed at 4.1 K and attribute it to local maxima  
10 near the Fermi level in the density of states.  
11  
12

13 The heat capacity of  $\text{Sm}_2\text{Ru}_3\text{Sn}_5$  is shown in Figure 3b. There is a sharp peak at 2.1 K,  
14 consistent with the antiferromagnetic transition from field cooled magnetic susceptibility  
15 measurement ( $T_N = 2.3$  K). The data was fit with a Lattice-Debye model. After subtraction  
16 of the lattice contribution, the magnetic contribution to the heat capacity ( $C_{\text{mag}}$ ) was  
17 integrated to find the magnetic entropy ( $S_{\text{mag}}$ ). The magnetic entropy saturates at a value  
18 of  $R\ln(2)$ , consistent with a doublet ground state for the measured temperature range.  
19 This is lower than a full  $J = 5/2$  expected for a  $\text{Sm}^{3+}$  compound. A saturation of the  
20 magnetic entropy is observed for other  $\text{Sm}^{3+}$  compounds and is often attributed to crystal  
21 electric field effects caused by splitting of the  $f$  states.<sup>[29, 39-40]</sup>  
22  
23

#### 24. Electronic Structure

25 Figure 4 shows the band structure and density of states for  $\text{Ru}_3\text{Sn}_7$  and  $\text{Sm}_2\text{Ru}_3\text{Sn}_5$   
26 calculated with density functional theory (DFT). Both materials are metals, in agreement  
27 with the measured resistivity. The DOS near the Fermi energy of both materials is mainly  
28 composed of Ru  $d$  and Sn  $p$  orbitals, while the Sm atoms contribute little to the DOS of  
29  $\text{Sm}_2\text{Ru}_3\text{Sn}_5$ .  
30  
31  
32  
33  
34  
35  
36  
37  
38  
39  
40  
41  
42  
43  
44  
45  
46  
47  
48  
49  
50  
51  
52  
53  
54  
55  
56  
57  
58  
59  
60  
61  
62  
63  
64  
65

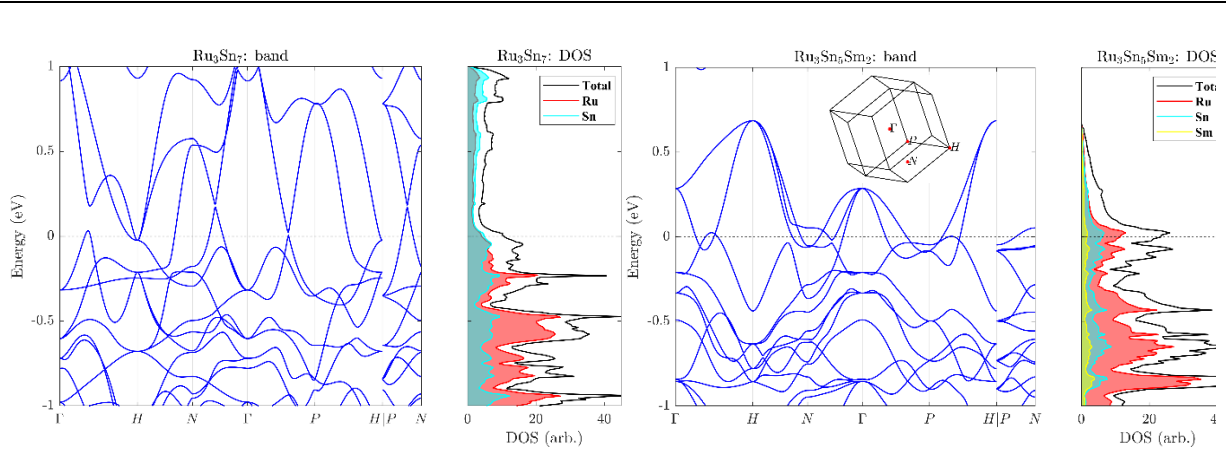


**Figure 4.** Band structure and density of state (DOS) of  $\text{Ru}_3\text{Sn}_7$  (left) and  $\text{Sm}_2\text{Ru}_3\text{Sn}_5$  (right), respectively. High-symmetry points in the Brillouin zone are shown in the inset of the  $\text{Sm}_2\text{Ru}_3\text{Sn}_5$  band structure panel. In the DOS plots, both the total and element-resolved DOSs are shown. The charge neutral point (Fermi energy) is set to zero energy.

The local density approximation with dynamical mean-field theory (LDA+DMFT) calculations support the localized picture ( $\text{Sm}^{3+}$ ) of the  $f$  electrons in the measured range of temperatures. Figure 5a displays the local density of states at  $T = 600$  K, and the total density of states. The  $f$  electrons are in a Mott state with fluctuating local moments and no weight at the Fermi level: The local density of states of the  $f$  electrons displays Hubbard bands in the one electron spectra. Figure 5b displays the probability distribution of the electronic configurations with different numbers of  $f$  electrons. The dominant occupation is  $\text{Sm}^{3+}$  with  $N = 5$  electrons, an open shell with a local fluctuating moment. In this material the conduction electrons are scattered by the local moments, and this additional scattering channel provides a possible explanation for the much larger value of the high

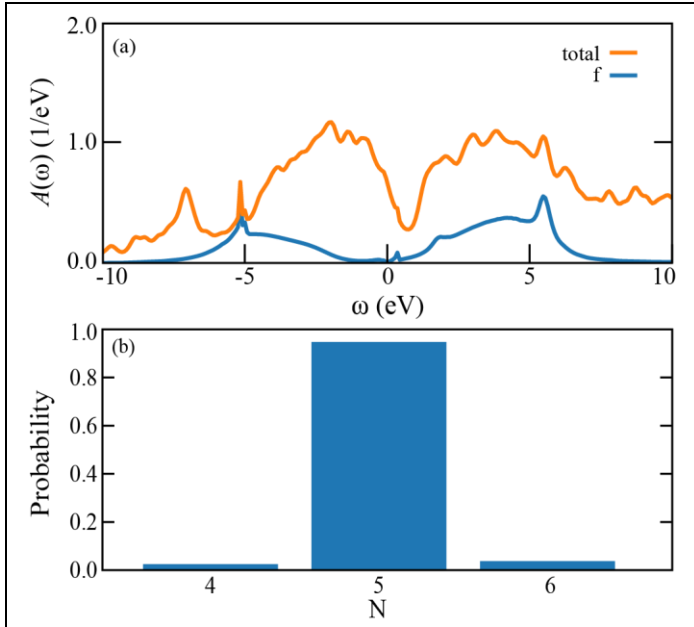


**Figure 5.** Spectral functions and valence histogram in  $\text{Sm}_2\text{Ru}_3\text{Sn}_5$  as predicted within one-shot LDA+DMFT at  $T = 600$  K. There is no  $\text{Sm}-f$  character on the Fermi surface and the valence is almost always in the  $N = 5$

1  
2  
3  
4 temperature resistivity of  $\text{Sm}_2\text{Ru}_3\text{Sn}_5$  relative to  $\text{Ru}_3\text{Sn}_7$ . These local moments can be  
5 partially Kondo screened at lower temperatures, as it has been observed, for example, in  
6  $\text{UGe}_2$ .<sup>[41]</sup> This could account for the reduced magnetic entropy observed in the heat  
7 capacity (Figure 3). In this picture, one can interpret the scale of  $\theta_{\text{CW}} = -36.6$  K extracted  
8 from the susceptibility as a Kondo scale.  
9  
10  
11  
12  
13

### 14 3. Conclusions

15  
16  
17  
18  
19  
20  
21  
22  
23  
24  
25  
26  
27  
28  
29  
30  
31  
32  
33  
34  
35  
36  
37  
38  
39  
40  
41  
42  
43  
44  
45  
46  
47  
48  
49  
50  
51  
52  
53  
54  
55  
56  
57  
58  
59  
60  
61  
62  
63  
64  
65

We have successfully prepared  $\text{Sm}_2\text{Ru}_3\text{Sn}_5$  and measured its physical properties. Our joint experimental and computational methods support localized Sm *f* electrons. An antiferromagnetic transition is observed at  $T_N = 3.8$  K, and our DFT and LDA+DMFT calculations indicate a dominant  $\text{Sm}^{3+}$  occupation of the electronic configuration probability distribution. Based on the local density of states ( $T = 600$  K), the *f*-electrons are in a Mott state indicating the presence of Hubbard bands. Notably, the  $\theta_{\text{CW}}$  is an order of magnitude larger than the ordering temperature implying either geometric frustration of the magnetic moments or partial Kondo screening of the Sm magnetic moments at low temperatures. Our analysis of the heat capacity for  $\text{Sm}_2\text{Ru}_3\text{Sn}_5$  is consistent with a doublet ground state, implying the presence of crystal field effects which could artificially inflate  $\theta_{\text{CW}}$  and impact the frustration parameter. The geometric frustration could be explained by the tetrahedral Sm sublattice; however, other measurements indicate possible screening of the local Sm moments by the conduction electrons. The reduced moment of approximately  $0.06 \mu_B/\text{Sm}$  in  $\text{Sm}_2\text{Ru}_3\text{Sn}_5$  can be attributed to partial screening of localized magnetic moments by conduction electrons. For comparison,  $\text{SmPd}_2\text{Al}_3$  (where Sm also carries a  $\text{Sm}^{3+}$  moment) shows a lower than expected magnetic moment of  $0.16 \mu_B/\text{Sm}$  due to strong crystal field effects.<sup>[30]</sup> Transport measurements of  $\text{Sm}_2\text{Ru}_3\text{Sn}_5$  indicated a higher resistivity than  $\text{Ru}_3\text{Sn}_7$ . This could be explained by local Sm magnetic moments contributing to the scattering of the conduction electrons.

Given the interest in  $\text{SmB}_6$  (a topological Kondo insulator) and  $\text{SmCoIn}_5$  (an antiferromagnet with Kondo screening), low-temperature resistivity measurements to probe  $\text{Sm}_2\text{Ru}_3\text{Sn}_5$  for a Kondo resonance would be very useful in confirming Kondo screening of the Sm moments in  $\text{Sm}_2\text{Ru}_3\text{Sn}_5$ . Our joint experimental and computational methods suggest the presence of Hubbard bands, making it worthwhile to explore the

1  
2  
3  
4 possibility of suppressing magnetism to observe a Kondo lattice. Given the nature of the  
5 magnetism, inelastic X-ray scattering measurements would also be useful in  
6 experimentally confirming the electronic structure or the Fermi surface of  $\text{Sm}_2\text{Ru}_3\text{Sn}_5$ .  
7 The competition between RKKY-type interactions and Kondo behavior opens exciting  
8 possibilities for studying topology and discovering new quantum materials to explore  
9 complex physical phenomena.  
10  
11  
12  
13  
14

15 **4. Experimental Methods**  
16  
17

18  $\text{Sm}_2\text{Ru}_3\text{Sn}_5$  was prepared via arc-melting. Stoichiometric ratios of the elements were  
19 measured and pressed together in a hydraulic press to create a homogeneous  
20 environment and prevent Ru powder from coating the interior of the setup. The elements  
21 were melted into a single boule under a positive flow of Ar gas. A Zr “getter” was included  
22 in the reaction setup to minimize oxidation of the sample. The boule was flipped and re-  
23 melted three times for homogeneity. Single-crystals were isolated from a fragment of the  
24 arc-melted boule (approximately  $0.01 \times 0.01 \times 0.02$  mm) and used to collect X-ray  
25 diffraction data at  $T = 160$  K and  $298$  K (above and below the previously reported  
26 temperature of  $T = 240$  K).<sup>[18]</sup> Data was collected using a Bruker D8 Quest Kappa single-  
27 crystal X-ray diffractometer equipped with an Incoatec  $1\mu\text{S}$  microfocus source (Mo  $\text{K}_\alpha$   
28 radiation,  $\lambda = 0.71073$  Å) and a PHOTON III CPAD area detector. The raw frames were  
29 integrated with Bruker SAINT, and the intensities were corrected for absorption with a  
30 multi-scan method in SADABS.<sup>[42]</sup> The intrinsic phasing method in SHELXT was used to  
31 generate preliminary crystallographic models,<sup>[43]</sup> which were finalized with least-squares  
32 refinements in SHELXL.<sup>[44]</sup> The details of the data collection, refinement parameters, and  
33 atomic coordinates are described in Tables 1 and 2.  
34  
35  
36  
37  
38  
39  
40  
41  
42  
43  
44  
45  
46  
47

48 Pieces of the arc-melted boule were also ground in an agate mortar and pestle. The  
49 powder was then placed on a low-background sample holder, and the powder X-ray  
50 diffraction data were collected on a Bruker D2 Phaser equipped with a Cu  $\text{K}_\alpha$  source ( $\lambda =$   
51  $1.54184$  Å) and a LYNXEYE XE-T detector. Data were collected in the  $2\theta$  range  $5 - 80$  °  
52 at room temperature and were analyzed by a Pawley fit in TOPAS (shown in Figure S1).<sup>[45]</sup>  
53  
54  
55  
56  
57  
58  
59  
60  
61  
62  
63  
64  
65

1  
2  
3  
4 Energy-dispersive X-ray spectroscopy (EDS) was performed on a piece of the arc-melted  
5 boule with a VERSA 3D focused ion beam scanning electron microscope. The formula  
6 obtained from EDS was  $\text{Sm}_{1.9(5)}\text{Ru}_{3.1(4)}\text{Sn}_{5.0(2)}$ , in good agreement with the nominal  
7 composition.  
8  
9

10  
11 Temperature-dependent magnetization data were collected on polycrystalline  $\text{Sm}_2\text{Ru}_3\text{Sn}_5$   
12 using a Quantum Design MPMS system. The sample was zero-field-cooled (ZFC), then  
13 measured on warming from 1.8 – 300 K in an external magnetic field of 0.1 T. The field-  
14 dependent magnetization data were collected at 1.8 K in a range -7 – 7 T. The electrical  
15 resistance and heat capacity were measured on the same sample in a Quantum Design  
16 PPMS system. For the electrical resistance, a standard 4-probe method was employed  
17 on the same sample, where each probe consisted of 0.002 in. diameter Pt wire attached  
18 with silver paste. A current of 500  $\mu\text{A}$  was applied, and resistance was measured on  
19 cooling in a temperature range of 300 – 2 K.  
20  
21

22 The electronic structure was calculated using density functional theory (DFT) as  
23 implemented in the Vienna *Ab-initio* Simulation Package (VASP).<sup>[46]</sup> The Perdew, Burke,  
24 and Ernzerhof (PBE) generalized gradient approximation<sup>[47]</sup> was employed to model the  
25 electron exchange–correlation interactions. The Projected Augmented Wave (PAW)  
26 method<sup>[48]</sup> was utilized, treating the Sm *f* electrons as core states. All crystal structures  
27 were fully relaxed until the forces on all atoms were below 1 meV/Å. A plane-wave basis  
28 set with an energy cutoff of 300 eV was used. The reciprocal space was sampled using a  
29  $10 \times 10 \times 10$  k-point mesh. Spin–orbit coupling was not included. The density of states was  
30 calculated using the tetrahedron method with Blöchl corrections.  
31  
32

33 To calculate the electronic structure including correlation effects, we used codes in  
34 Comsuite.<sup>[49]</sup> In particular, we conducted one-shot density functional theory + dynamical  
35 mean field theory (DFT+DMFT) calculations using *Portobello*,<sup>[50]</sup> the all-electron code  
36 FlapwMBPT<sup>[49, 51-52]</sup> to solve the fully relativistic DFT problem within the local density  
37 approximation, and the continuous-time quantum Monte Carlo code ComCTQMC<sup>[53]</sup> to  
38 solve the quantum impurity problem. The Sm-4*f* shell is treated as correlated, and a  
39 spherically symmetric Slater-Condon interaction is applied with Hubbard interaction  $U =$   
40 6.5 eV and Hund interaction  $J = 0.7$  eV. We use the nominal double counting<sup>[54]</sup> with  
41  
42

1  
2  
3  
4 nominal occupancy  $N_0 = 5$  and conduct the calculations at 600 K. We then computed the  
5 spectral functions of the  $f$  electrons,  $A(\omega)$ , and the valence histogram, *i.e.*, the projection  
6 of the many-body density matrix onto the number of electrons,  $N$ .  
7  
8

9  
10 **Acknowledgements**  
11  
12

13 J.Y.C. gratefully acknowledges the support of both the Welch Foundation, AA-2056-  
14 20240404 and the U.S. Department of Energy, DE-SC0022854. A portion of this work was  
15 performed at the National High Magnetic Field Laboratory (NHMFL), which is supported  
16 by National Science Foundation Cooperative Agreement No. DMR-2128556 and the  
17 State of Florida. B.C.S. and K.W. acknowledge the support of the NHMFL User  
18 Collaboration Grant Program (UCGP). GK and CM were supported by the US Department  
19 of Energy, Office of Basic Energy Sciences as part of the Computation Material Science  
20 Program.  
21  
22

23  
24 **Accession Codes**  
25  
26

27 Crystallographic data (excluding structure factors) for the structures reported in this paper  
28 have been deposited with the Cambridge Crystallographic Data Centre as supplementary  
29 publication no. CSD-2421218 - 2421219. Copies of the data can be obtained free of  
30 charge on application to CCDC, 12 Union Road, Cambridge CB2 1EZ, UK [fax.: (internat.)  
31 + 44 1223/336-033; e-mail: [deposit@ccdc.cam.ac.uk](mailto:deposit@ccdc.cam.ac.uk)].  
32  
33  
34  
35  
36  
37  
38  
39  
40  
41  
42  
43  
44  
45  
46  
47  
48  
49  
50  
51  
52  
53  
54  
55  
56  
57  
58  
59  
60  
61  
62  
63  
64  
65

1  
2  
3  
4  
5  
6 References:

7 [1] M. Kasaya, B. Liu, M. Sera, T. Kasuya, D. Endoh, T. Goto, T. Fujimura, *J. Magn. Magn. Mater.* **1985**, 52, 289-292.

8 [2] U. Ahlheim, K. Fraas, P. H. P. Reinders, F. Steglich, O. Nakamura, T. Suzuki, T. Kasuya, *J. Magn. Magn. Mater.* **1992**, 108, 213-214.

9 [3] W. M. Williams, R. T. Macaluso, M. Moldovan, D. P. Young, J. Y. Chan, *Inorg. Chem.* **2003**, 42, 7315-7318.

10 [4] M. L. Fornasini, P. Manfrinettib, A. Palenzonab, S. K. Dharc, *Z. Naturforsch., B: Chem. Sci.* **2003**, 58, 521-527.

11 [5] M. Dzero, K. Sun, V. Galitski, P. Coleman, *Phys. Rev. Lett.* **2010**, 104, 106408.

12 [6] Y. Li, Q. Ma, S. X. Huang, C. L. Chien, *Sci. Adv.* **2018**, 4, eaap8294.

13 [7] C.-J. Kang, H. C. Choi, K. Kim, B. I. Min, *Phys. Rev. Lett.* **2015**, 114, 166404.

14 [8] C.-J. Kang, D.-C. Ryu, J. Kim, K. Kim, J. S. Kang, J. D. Denlinger, G. Kotliar, B. I. Min, *Phys. Rev. Mater.* **2019**, 3, 081201.

15 [9] D. W. Tam, N. Colonna, N. Kumar, C. Piamonteze, F. Alarab, V. N. Strocov, A. Cervellino, T. Fennell, D. J. Gawryluk, E. Pomjakushina, Y. Soh, M. Kenzelmann, *Commun. Phys.* **2023**, 6, 223.

16 [10] X. Yao, J. Gaudet, R. Verma, D. E. Graf, H.-Y. Yang, F. Bahrami, R. Zhang, A. A. Aczel, S. Subedi, D. H. Torchinsky, J. Sun, A. Bansil, S.-M. Huang, B. Singh, P. Blaha, P. Nikolić, F. Tafti, *Physical Review X* **2023**, 13, 011035.

17 [11] W. K. Brown, M. A. Plata, M. E. Raines, J. Y. Chan, in *Handbook on the Physics and Chemistry of Rare Earths*, Vol. 64 (Eds.: J.-C. G. Bunzli, S. M. Kauzlarich), Elsevier, **2023**, pp. 1-92.

18 [12] L. Chen, C. Setty, H. Hu, M. G. Vergniory, S. E. Grefe, L. Fischer, X. Yan, G. Eguchi, A. Prokofiev, S. Paschen, J. Cano, Q. Si, *Nat. Phys.* **2022**, 18, 1341-1346.

19 [13] T. M. Kyrk, E. R. Kennedy, J. Galeano-Cabral, G. T. McCandless, M. C. Scott, R. E. Baumbach, J. Y. Chan, *Sci. Adv.* **2024**, 10, eadl2818.

20 [14] G. Venturini, M. Méot-Meyer, J. F. Marêché, B. Malaman, B. Roques, *Mater. Res. Bull.* **1986**, 21, 33-39.

21 [15] D. E. Bugaris, C. D. Malliakas, F. Han, N. P. Calta, M. Sturza, M. J. Krogstad, R. Osborn, S. Rosenkranz, J. P. C. Ruff, G. Trimarchi, S. L. Bud'ko, M. Balasubramanian, D. Y. Chung, M. G. Kanatzidis, *J. Am. Chem. Soc.* **2017**, 139, 4130-4143.

22 [16] R. Sokkalingam, G. Lingannan, M. Sundaramoorthy, C. S. Lue, C. N. Kuo, B. Joseph, S. Arumugam, *Solid State Commun.* **2023**, 372, 115293.

23 [17] C. N. Kuo, C. J. Hsu, C. W. Tseng, W. T. Chen, S. Y. Lin, W. Z. Liu, Y. K. Kuo, C. S. Lue, *Phys. Rev. B* **2020**, 101, 155140.

24 [18] V. Pavlova, E. Murashova, *Z. Kristallogr. Cryst. Mater.* **2021**, 236, 137-145.

25 [19] O. Nial, *Sven. Kem. Tidskr* **1947**, 59, 172-177.

26 [20] A. Flessa Savvidou, A. Ptok, G. Sharma, B. Casas, J. K. Clark, V. M. Li, M. Shatruk, S. Tewari, L. Balicas, *npj Quantum Mater.* **2023**, 8, 68.

[21] U. Häussermann, M. Elding-Pontén, C. Svensson, S. Lidin, *Chem. Eur. J.* **1998**, *4*, 1007-1015.

[22] L. Eriksson, J. Lanner, *Acta Crystallogr. E*. **2001**, *57*, i85-i86.

[23] C.-W. Wang, S. K. Karna, S.-i. Yano, C.-H. Lee, M. Avdeev, C. S. Lue, C. N. Kuo, *Phys. Rev. B* **2022**, *105*, 104429.

[24] D. Swenson, *MRS Online Proceedings Library* **1996**, *453*, 367-372.

[25] V. J. Yannello, B. J. Kilduff, D. C. Fredrickson, *Inorg. Chem.* **2014**, *53*, 2730-2741.

[26] V. J. Yannello, D. C. Fredrickson, *Inorg. Chem.* **2015**, *54*, 11385-11398.

[27] Y. Li, S. M. Winter, D. A. S. Kaib, K. Riedl, R. Valentí, *Phys. Rev. B* **2021**, *103*, L220408.

[28] L. Savary, L. Balents, *Rep. Prog. Phys.* **2017**, *80*, 016502.

[29] J. Pospíšil, M. Kratochvílová, J. Prokleška, M. Diviš, V. Sechovský, *Phys. Rev. B* **2010**, *81*, 024413.

[30] J. Pospíšil, G. Nénert, S. Miyashita, H. Kitazawa, Y. Skourski, M. Diviš, J. Prokleška, V. Sechovský, *Phys. Rev. B* **2013**, *87*, 214405.

[31] A. P. Ramirez, *Annu. Rev. Mater. Res.* **1994**, *24*, 453-480.

[32] S. Mugiraneza, A. M. Hallas, *Commun. Phys.* **2022**, *5*, 95.

[33] M. A. Ruderman, C. Kittel, *Phys. Rev.* **1954**, *96*, 99-102.

[34] T. Kasuya, *Prog. Theor. Phys.* **1956**, *16*, 45-57.

[35] J. Kondo, *Prog. Theor. Phys.* **1964**, *32*, 37-49.

[36] A. C. Hewson, *The Kondo Problem to Heavy Fermions*, Cambridge University Press, **1997**.

[37] B. C. Chakoumakos, D. Mandrus, *J. Alloys Compd.* **1998**, *281*, 157-159.

[38] C. Lv, X. Cheng, J. Sui, K. Jia, X. Dong, M. Ding, B. Pan, *Phys. B: Condens.* **2024**, *677*, 415733.

[39] V. V. Novikov, N. V. Mitroshenkov, A. V. Matovnikov, *J. Alloys Compd.* **2015**, *646*, 906-911.

[40] K. Feng, C. Bush, O. Oladehin, M. Lee, R. Baumbach, *Phys. Rev. B* **2024**, *109*, 014436.

[41] I. Giannakis, D. Sar, J. Friedman, C.-J. Kang, M. Janoschek, P. Das, E. D. Bauer, G. Kotliar, P. Aynajian, *Phys. Rev. Res.* **2022**, *4*, L022030.

[42] L. Krause, R. Herbst-Irmer, G. M. Sheldrick, D. Stalke, *J. Appl. Crystallogr.* **2015**, *48*, 3-10.

[43] G. Sheldrick, *Acta Crystallogr. A*. **2015**, *71*, 3-8.

[44] G. Sheldrick, *Acta Crystallogr. C*. **2015**, *71*, 3-8.

[45] A. Coelho, *J. Appl. Crystallogr.* **2018**, *51*, 210-218.

[46] G. Kresse, J. Furthmüller, *Comput. Mater. Sci* **1996**, *6*, 15-50.

[47] J. P. Perdew, K. Burke, M. Ernzerhof, *Phys. Rev. Lett.* **1996**, *77*, 3865-3868.

[48] P. E. Blöchl, *Phys. Rev. B* **1994**, *50*, 17953-17979.

1  
2  
3  
4 [49] S. Choi, P. Semon, B. Kang, A. Kuteпов, G. Kotliar, *Comput. Phys. Commun.* **2019**,  
5 244, 277-294.  
6  
7 [50] R. Adler, C. Melnick, G. Kotliar, *Comput. Phys. Commun.* **2024**, 294, 108907.  
8  
9 [51] A. L. Kuteпов, V. S. Oudovenko, G. Kotliar, *Comput. Phys. Commun.* **2017**, 219,  
10 407-414.  
11  
12 [52] A. L. Kuteпов, *Phys. Rev. B* **2021**, 103, 165101.  
13  
14 [53] C. Melnick, P. Sémond, K. Yu, N. D'Imperio, A.-M. Tremblay, G. Kotliar, *Comput.*  
15 *Phys. Commun.* **2021**, 267, 108075.  
16  
17  
18  
19  
20  
21  
22  
23  
24  
25  
26  
27  
28  
29  
30  
31  
32  
33  
34  
35  
36  
37  
38  
39  
40  
41  
42  
43  
44  
45  
46  
47  
48  
49  
50  
51  
52  
53  
54  
55  
56  
57  
58  
59  
60  
61  
62  
63  
64  
65

[54] K. Haule, C.-H. Yee, K. Kim, *Phys. Rev. B* **2010**, 81, 195107.